The 5th Asia Conference on Earthquake Engineering
October 16-18, 2014

TESTING AND MODELING OF A36 AND STAINLESS STEEL BUCKLING-RESTRAINED BRACES UNDER NEAR-FAULT LOADING CONDITIONS

Joel Lanning[1] and Chia-Ming Uang[2]

ABSTRACT

This paper summarizes results from a research project including a testing program of six full-scale buckling-restrained braces (BRBs). These braces were subjected to large-amplitude loading protocols, statistically representing deformation demands obtained from a suite of near-fault ground motions applied to a finite element model of a long-span bridge. Four BRBs possessed stainless steel (SS) yielding cores and two BRBs used conventional mild steel yielding cores. All BRBs performed well under the severe loading, demonstrating the ability of BRBs to sustain multiple consecutive near-fault protocols. Two BRBs, one of each steel type, were tested dynamically to study the strain rate effect. A summary is provided of the increase in brace force due to the significant strain hardening properties of SS and due to high strain rate, which was observed of both steel types. Further, the large nonsymmetrical loading results made clear the inconsistencies between current BRB prequalifying testing procedures, design assumptions, and actual BRB seismic force effects for capacity design. An alternative testing method is proposed. For numerical simulation of BRB response, a commonly used bilinear model is shown to be insufficient, especially for large nonsymmetrical loading like that experienced by structures near seismic faults. A modified Menegotto-Pinto material model is shown to provide excellent correlation to test results when the following features are incorporated: (1) a larger post-yield stiffness in compression than in tension, (2) an appropriate isotropic hardening relation for SS BRB which includes the effect of cumulative ductility, (3) the strain rate effect.

Keywords: buckling-restrained brace, near-fault ground motion, mild steel, stainless steel, cyclic modeling

TEST PROGRAM

Introduction

Buckling-restrained braces (BRBs) are an attractive energy dissipation device due to their excellent cyclic inelastic capacity, simple construction, and low maintenance requirements. Primarily they consist of a yielding steel core surrounded by, and de-coupled from, concrete mortar within a hollow structural section, as shown in Fig. 1(a) along with a schematic representation of the typical stable hysteretic response. As the yielding core of a BRB (with a yield length L_y in Fig. 2) experiences multiple inelastic excursions, the material undergoes strain hardening and causing the brace force to exceed the initial yield force. Furthermore during compression excursions, Poisson expansion and restrained high-mode inelastic buckling of the yielding core result in contact friction between the core and the restraining assembly. Consequently, compression forces are somewhat larger than tension forces at equal and opposite deformations. Hence, for capacity design a crucial aspect of AISC Seismic Provisions (AISC 341) BRB qualification testing is the determination of the compression strength adjustment factor, β, shown in Fig. 1(b) along with the tension strength adjustment factor, ω. The value of β is limited to 1.3 in AISC 341 (AISC 2010), as measured within each of the symmetric cycles of the AISC loading protocol (Fig. 3c) from a single BRB test, in an attempt to regulate the unbalanced brace forces making BRBs more amenable to capacity based design of the adjoining structural members.

[1] Assistant Professor, California State University, Fullerton, CA 92831, USA, joellanning@fullerton.edu
[2] Professor, University of California, San Diego, La Jolla, CA 92093, USA, cmu@ucsd.edu

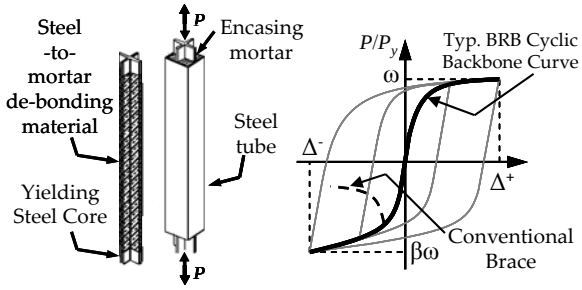

Figure 1. (a) Basic BRB anatomy; (b) schematic BRB hysteretic response

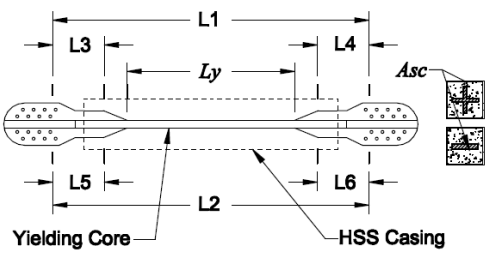

Figure 2. Specimen dimensions

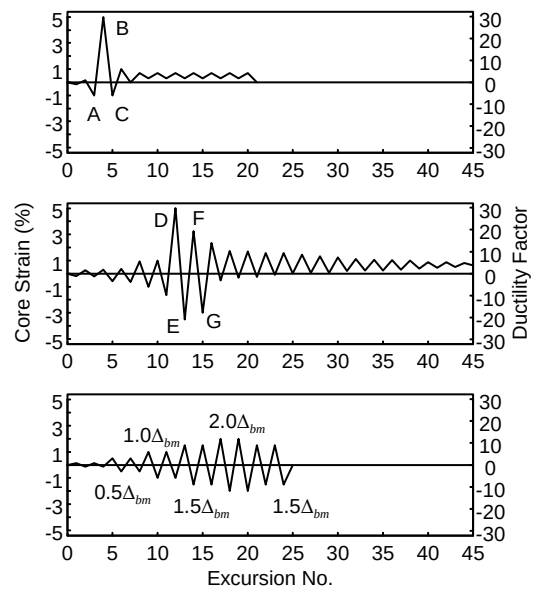

Figure 3. Pseudo-static Protocols
(a) VTB Proof; (b) Near Fault; (c) AISC

As part of a research project (Lanning et al, 2013) investigating the feasibility of utilizing BRBs on long-span bridges near seismic faults, the Vincent Thomas Bridge (VTB) in Southern California served as a useful case study and model bridge for determining appropriate deformation demands on BRBs. The suspended spans of the VTB connect San Pedro to Long Beach, California, causing the bridge to be situated along the pacific coast and directly over the Palos Verdes Fault. These circumstances are common for many long-span bridges in California, and therefore this scenario presents an important new structural application and seismic environment for BRBs.

Near-Fault Loading Protocols

Protocols for long-span bridge BRBs were developed with brace axial deformation demands obtained from subjecting a finite element model of the VTB to a pre-established site-specific design earthquake together with a suite of 17 other near-fault ground motions. All were scaled to the design earthquake spectrum representing a 3.8% chance of exceedance over the 125-year remaining bridge service life. The resulting cyclic demands make up the Proof Protocol (Pr) and the Near Fault (NF) Protocol, shown in Fig. 3(a) and (b), respectively, which are large amplitude, asymmetric, and contain high strain rates. Each of these characteristics is neglected in the only existing BRB provisions of AISC 341. Furthermore, the AISC Protocol, in Fig. 3(c), consists of symmetric and relatively small amplitude cycles, and represent the BRB deformation demands within building frames excited by far-field ground motion (Sabelli et al. 2003). All three protocols were utilized in this test program with peak strain in either direction, as indicated in Table 1 by "-T" or "-C" for tension and compression directions, respectively. Dynamic versions were also developed but are not shown for brevity.

Specimens and Setup

A total of six full-scale BRBs comprised two sets of three geometrically identical braces. The six yielding cores were fabricated from four steel plates; cores of Specimens 1 through 4 were made from two ASTM A240 Type 304/304L stainless steel (SS) plates, while those of Specimens 4 and 5 were of two A36 steel plates. Specimen dimensions and properties are shown in Fig. 2 and quantified in Table 1 along with their testing sequences. The authors independently conducted tensile coupon tests of the SS plates at pseudo-static and high strain rates (= 0.25in/in/sec or 25% sec^{-1}). Results were consistent with those observed by Nordberg (2004) in that the yield stress increased by approximately 20%, while the ultimate strength decreased by about 10% when monotonically loaded at this high rate.

Table 1. BRB specimen designation and loading characteristics

Spec. No.	Test Order	Core Plate				BRB		Load Rate[b]	Test Sequence and Loading Protocol				Max. Core Strain (%)	η	ψ_h
		Steel Grade	Shape[a]	A_{sc} (cm²)	L_y (m)	P_{ya} (kN)	Δ_{by} (mm)		1st	2nd	3rd	4th	Tens. (Comp.)		
1	1	SS	+	103	3.2	2,808	5.8	PS	Pr-T	Pr-C[c]	n/a	n/a	4.7 (2.6)	112[c]	133[c]
2	2					2,370	5.1	PS	Pr-C	NF-T	AISC	n/a	4.6 (5.1)	724	1,024
3	4		–	52	3.8	1,186	5.6	D	Pr-C	NF-C	AISC	LCF[d]	3.7 (5.5)	1,221	2,052
4	5					1,404	6.6	PS	Pr-C	NF-C	AISC	n/a	3.8 (5.4)	820	1,177
5	3	A36	+	103	3.2	2,946	5.8	PS	NF-T	NF-C	n/a	n/a	5.0 (4.8)	747	859
6	6		–	52	3.8	1,459	6.6	D	Pr-C	NF-C	AISC[e]	n/a	3.7 (5.4)	733	888

[a] "+" and "–" designate cruciform and flat plate cross-section, respectively; [b] "PS" and "D" designate pseudo-static and dynamic loading rates, respectively; [c] Specimen 1 experienced a gusset connection instability; [d] Low-cycle fatigue protocol, fracture occurred: [e] Fracture occurred

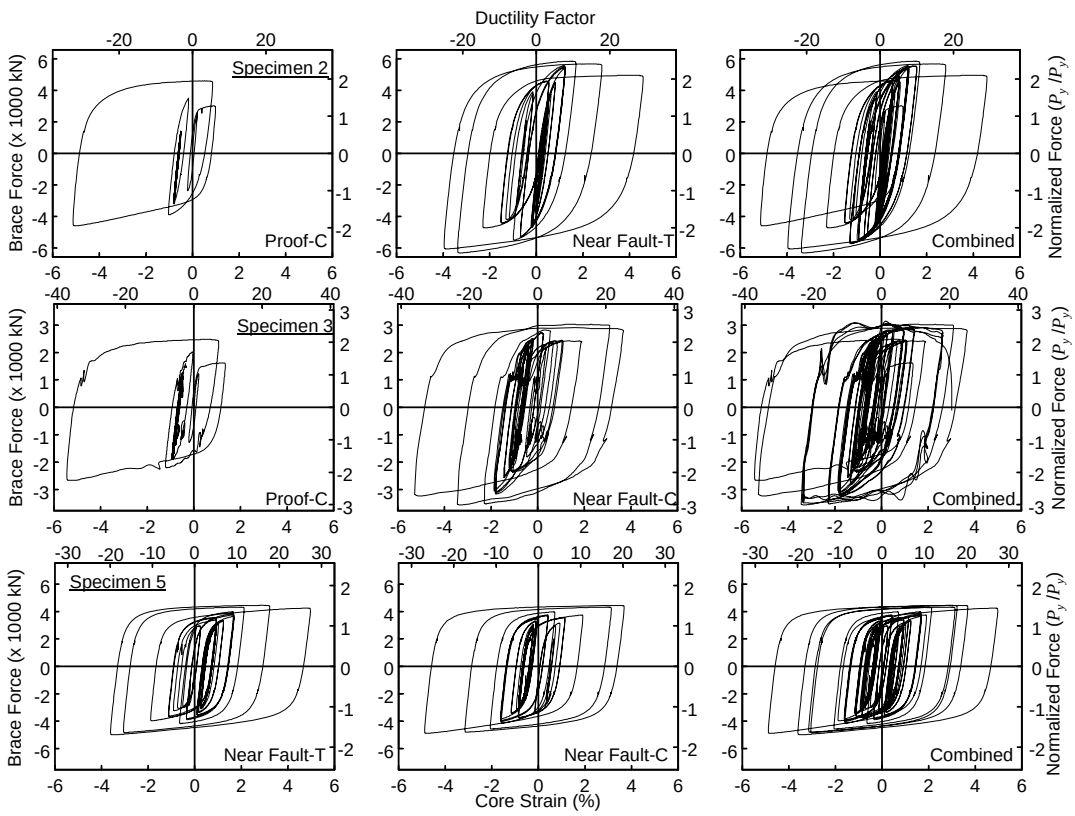

(a) (b) (c)

Figure 4. Hysteretic response of test specimens: (a) 1st test; (b) 2nd test; (c) All tests combined

Uniaxial deformations were applied to the specimens at the Seismic Response Modification Device (SRMD) facility at the University of California, San Diego. A redundant set of string potentiometers, labeled L1 through L6 in Fig. 2, were used measure the core deformation. Brace forces were measured by the load cell in each of the four actuators driving the SRMD shake table. Video was recorded for each test specimen; several videos are provided on the internet (YouTube, Lanning et al. 2014).

Overall Performance

All braces performed well and withstood multiple subsequent protocols, resulting in multiple excursions of 5% core strain (see Specimen 1 in Table 1 for the only exception). Hysteretic performance of several specimens is displayed in Fig. 4, where brace deformation, Δ, is given in terms

of core strain, calculated over the length L_y, and as ductility factor found by normalizing Δ by the yield deformation Δ_{by}. Brace forces, P, are shown normalized by the respective actual yield force, P_{ya}. Each BRB sustained large cumulative inelastic ductility, η, well in excess of the typical AISC required value of 200 (see Table 1). This is an indication of the accumulated sustained material damage and is commonly approximated by finding sum of the normalized deformations:

$$\eta = \sum \frac{2\left|\Delta_i^+ - \Delta_i^-\right|}{\Delta_{by}} - 4 \tag{1}$$

where Δ_i^+ and Δ_i^- are the algebraic peak positive and negative deformations. In comparing the energy dissipation between specimens, the normalized dissipated energy is a better cross-specimen measure:

$$\psi_h = \frac{E_h}{P_{ya}\Delta_{by}} = \frac{\int P \cdot d\Delta}{P_{ya}\Delta_{by}} \tag{2}$$

where E_h is the total energy dissipated during the test. Both η and ψ_h values are summarized in Table 1. The superior energy dissipation and cumulative ductility capacity of SS BRBs are evident when comparing Specimens 3 and 6.

ANALYSIS OF TEST RESULTS

Large Nonsymmetrical Cycles and Proposed Qualification Testing Procedure

The conventional measurement of the unbalance between compression and tension BRB forces, depicted in Fig. 1, is measured as the ratio of subsequent peak compression (= $\beta\omega P_y$) and tension (=*ωP_y) forces during each of the symmetric cycles of the AISC Protocol applied to a single BRB. The primary reason for measuring the unbalanced force is to obtain the resultant between two opposing BRBs within a frame, like that shown in Fig. 5, for the capacity design of the member and gusset connection that both BRBs are connected to. However, this "β-method" is inconsistent with the actual seismic effects on the adjoining elements, as there are actually two braces at work, not a single BRB. Furthermore, AISC 341 assumes only one unbalanced force scenario in which the BRB in compression always exhibits a larger axial force than the one in tension. However, the highly nonsymmetrical cycles in near-fault simulation revealed a second resultant force case, as demonstrated by the few cycles of Specimens 1 and 2 in Fig. 5. (Note that the hysteretic plot is to scale, but units have been removed for sizing purposes.) Case 1 and Case 2 show a possible resultant in either direction.

Therefore, a new testing procedure is proposed in which two nominally identical BRBs are tested to equal but opposite loading protocols. Then, an *unbalanced force factor* may be computed at the *i*-th excursion as:

$$\gamma_i = \frac{\omega_{C,i}}{\omega_{T,i}} \tag{3}$$

where the *i*-th *compression* and *tension overstrength factors* are ω_{Ci} and ω_{Ti}, respectively, and are numerically equal to the peak force normalized by P_{ya}. Maximum ω_C and ω_T values in the two BRB tests provide the maximum individual brace compressive and tensile forces, respectively, to be utilized for the design of adjoining gusset connections and surrounding structural components. Further, the proposed testing procedure also reveals another unbalanced force case (Case 2 in Fig. 5) that should be considered in designing the beam, a scenario not considered in AISC 341.

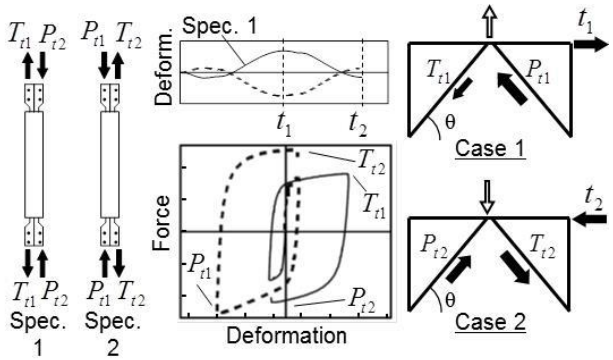

Figure 5. Proposed testing procedure and unbalanced force scenarios

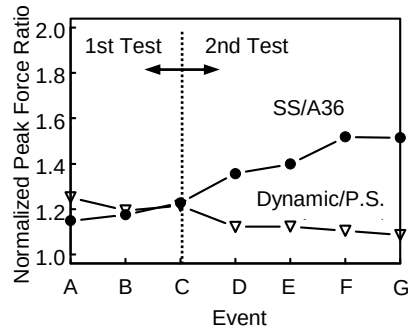

Figure 6. Increase in brace force due to yielding core material type and high strain rate

Effect of Yielding Core Steel Type

The geometrically identical Specimens 3 (SS) and 6 (A36) were subjected to the same dynamic loading protocols with equal strain magnitudes, and both were tested to fracture. The superior ductility capacity and energy dissipation capability of SS is displayed by Specimen 3, which sustained η of 1.67 and ψ_h of 2.31 times greater than Specimen 6 (Table 1). However, the desirable corrosion resistance and cumulative ductility capability of SS, Type 304/304L among other grades, is accompanied by significantly different strain hardening behavior as compared to A36 steel. Fig. 6 provides a summary of SS-to-A36 peak overstrength ratios from significant events A through G as shown in Fig. 3. The ratio is observed to grow quite large, with an average value of 1.2 and a maximum of 1.5.

The substantially greater isotropic cyclic strain hardening behavior (dilation of the yield surface) of SS is well known, as shown by Paul et al. (2010) among others, while cyclic tests on A36 steel coupons by Kaufmann et al. (2001) show its hardening to be mostly kinematic (translation of the yield surface) in nature with much less isotropic tendency. This is an important feature to consider when specifying BRBs with SS yielding cores as a reliable estimate of the maximum force that can be developed in a BRB is critical for capacity design.

Effect of Strain Rate

Mild structural steels such as A36 are generally assumed as rate-independent because the yield stresses are typically only about 7% higher under seismic loading rates (Di Sarno et al. 2002). SS is recognized as more strain-rate-dependent, as summarized by Nordberg (2004) with flow stresses (stress required to continue deforming plastically) at both 0.2% and 2% strains approximately 1.3 times greater due to an increase in strain rate from 0.1% to 100% sec^{-1}. However, little test data was available including BRBs subjected to large amplitude high strain rate excursions. It was suspected that the complex restrained inelastic buckling of the BRB core may exhibit a strain rate dependence.

Therefore, nominally identical SS Specimens 3 and 4 were subjected to the same protocols, but with dynamic and pseudo-static loading rates, respectively. Again, Fig. 6 shows a summary of the dynamic-to-pseudo-static peak overstrength ratios. The average ratio of about 1.2 clearly demonstrates a relatively significant strain rate effect on BRB, with a similar trend present for comparable A36 BRBs as well. This additional overstrength should not be neglected in capacity design for near-fault BRB applications.

NUMERICAL SIMULATION

Correlation of Bilinear Truss Element

A simple bilinear truss element has been used by many researchers (Sabelli et al., 2003, and Ravi et al., 2007, among others) which possesses a non-zero post-yield stiffness and a kinematic hardening

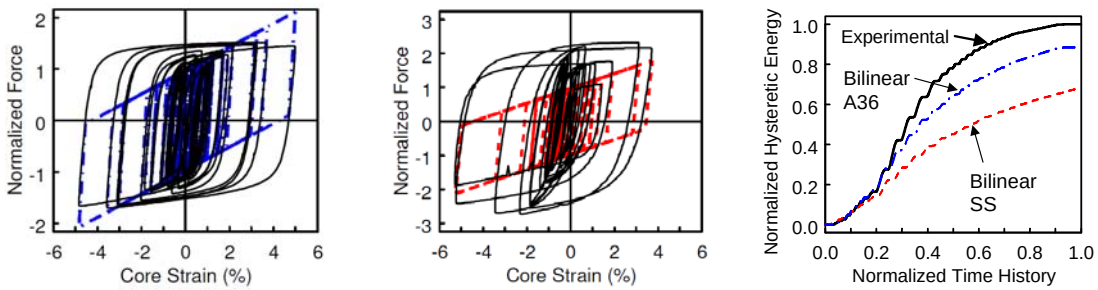

(a) (b) (c)

Figure 7. Bilinear BRB simulation of near-fault protocol test results: (a) Specimen 5 (A36); (b) Specimen 4 (SS); (c) comparison of dissipated energy.

rule. This model correlates reasonably well when compared to typical A36 yielding core specimen test results, which contain relatively small amplitude symmetric cycling. However, the deficiencies of this model in representing BRBs were highlighted in this research due to the large amplitude cycles and especially the use of SS.

Fig. 7 displays the comparison between the bilinear model and test results. The bilinear model possessed a post-yield stiffness equal to 3.25% of the initial elastic stiffness of the BRB, which is within the typical range in the literature. For A36 and SS BRB, respectively, the bilinear element clearly overestimates and drastically underestimates the peak forces, shown in Fig. 7(a) and (b). For both specimens the model underestimates the dissipated energy, in Fig. 7(c), with SS resulting in approximately 40% error. The bilinear model lacks representation of the Bauschinger region and the isotropic hardening behavior of steel materials. The former affects both A36 and SS accuracy to relatively the same extent, while the latter causes a significant force misrepresentation for SS BRBs.

Menegotto-Pinto Material Model

The popularity of the smooth hysteretic model proposed by Menegotto and Pinto (1973) is due its simplicity and relatively high computational efficiency, while providing good representation of the hysteretic response of steel. The model was originally developed for characterizing reinforcing steel in concrete structures subjected to earthquake loading and is widely used within nonlinear structural analysis software like the OpenSees finite element system (OpenSees, McKenna et al. 2010) as the uniaxial material model *Steel02*. Stress is related directly to strain as follows in the normalized stress-strain coordinate system, where:

$$\sigma^* = b\varepsilon^* + \frac{(1-b)\varepsilon^*}{\left(1+\varepsilon^{*R}\right)^{1/R}} \tag{4}$$

$$\varepsilon^* = \frac{\varepsilon - \varepsilon_r}{\varepsilon_o - \varepsilon_r} \tag{5}$$

$$\sigma^* = \frac{\sigma - \sigma_r}{\sigma_o - \sigma_r} \tag{6}$$

The coordinate (ε_o, σ_o) is the intersection point of the elastic, E_o, and post-yield, E_2, moduli, updated with each strain reversal. One primary advantage of using the Menegotto-Pinto (MP) model is that it provides a smooth curve between the elastic, E_o, and post-yield, E_2, moduli, through the empirical parameter R. The parameter b is the ratio between the two slopes (= E_2/E_o). The transition region parameter, R, is given by the relation:

$$R_i = R_o - \frac{R_1 \xi_i}{R_2 + \xi_i} \tag{7}$$

R_o, R_1, and R_2 in the above equation are empirically found, and ξ_i is the previous excursion ductility measurement:

$$\xi_i = \frac{\varepsilon_{p,\max} - \varepsilon_{o,i}}{\varepsilon_y} \tag{8}$$

for the *i*-th excursion where $\varepsilon_{p,max}$ is the previously attained largest magnitude compressive and tensile strains, recorded separately, and $\varepsilon_{o,i}$ is the strain coordinate of the updated intersection point between the initial and post yield slopes. Another advantage of using the MP model is its ability to capture both kinematic and isotropic cyclic hardening type behaviors. However, the original formulation, developed by Filippou et al. (1983), was found to still lack features needed to most accurately represent the BRB response observed in this testing program.

MP Modifications for BRB

A modified isotropic hardening relationship was found to better represent the stress shift, σ_{sh}, observed in both A36 and SS; this was necessary to capture the SS behavior. The shift applied to the updated coordinate (ε_o, σ_o), thereby shifting the stress-strain curve, to account for the isotropic hardening for a given excursion, and is given as:

$$\sigma_{sh} = \sigma_y \left[a_1 \left(\frac{\varepsilon_{\max} - \varepsilon_{\min}}{2\varepsilon_y} \right)^{a_2} - a_3 \eta \right] \tag{9}$$

where σ_y is the yield stress, and the parameters a_1 through a_3 are found by correlation to test data. The total ductility achieved in the loading history drives this value, and is corrected with accumulated damage.

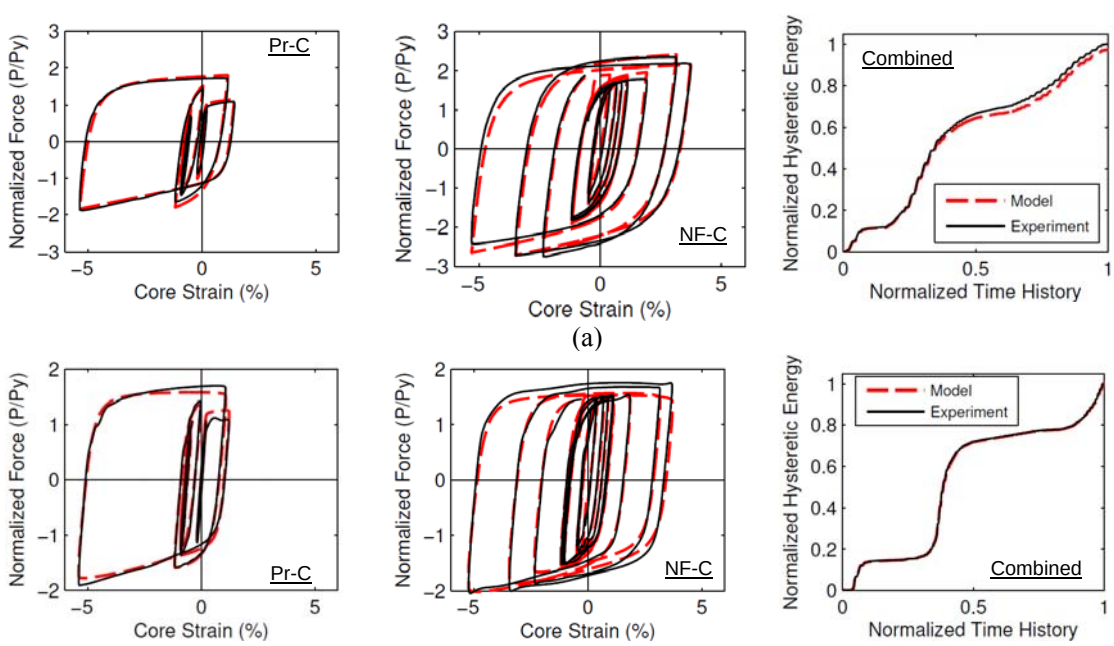

Figure 8. Modified Menegotto-Pinto BRB model versus test results: (a) Specimen 4; (b) Specimen 6

As mentioned above, the compression force in a BRB is typically larger than that in tension for a given magnitude of axial deformation. Therefore, it is necessary to go beyond the current practice of specifying a single parameter b by expanding the MP model to account for a tension post-yield slope, b_T, and a compression post-yield slope, b_C, separately. In this study, relations were found from the test data describing b_C and b_T; these followed the same equation form as R, in Eq. 7, with similar proportioning parameters, but with b_C being numerically equal to 4 times b_T.

Finally, the increased BRB stress due to the instantaneous strain rate was reflected by amplifying the rate independent algorithmic stress, σ, output by the *strain-rate amplification factor*, ω_{dyn}, found as:

$$\omega_{dyn} = \frac{\sigma_{dyn}}{\sigma_{PS}} = SR_1\dot{\mu} + SR_2\dot{\mu}^{SR_3} + SR_4\mu \tag{10}$$

where SR_1 through SR_4 are parameters fitting the equation to the testing data. A reduction was found to be necessary to be consistent with the decrease in strain rate dependence with accumulated inelastic deformation, η, especially for SS (Di Sarno et al., 2003). This reduction was, again, empirically determined as:

$$R_\eta = \eta^{SR_5} - SR_6\eta \tag{11}$$

with SR_5 and SR_6 obtained from testing. Therefore, the dynamic BRB stress is given as:

$$\sigma_{dyn} = \sigma\left(1 + \omega_{dyn}\right)R_\eta \tag{12}$$

With these modifications, excellent correlation to the testing data was achieved. Fig. 8 displays the simulated brace forces obtained with this modified MP model against pseudo-statically tested Specimen 4 and dynamically tested Specimen 6. It is evident that the peak forces, Bauschinger region, and dissipated energy are very well represented. Additionally, the modified MP model with strain rate effect properly simulated the response of pseudo-statically tested braces.

CONCLUSIONS

Application of near-fault loading protocols (Fig. 3), developed in this study, to six full-scale buckling-restrained braces demonstrated the ability of commercially available BRBs to withstand these severe deformations. The BRB response to the large-amplitude, nonsymmetrical cycles revealed the possibility of BRB tension forces being greater than BRB compression forces (Fig. 5) within the context of typical framing where these forces are from opposing BRBs with the frame. A consistent testing procedure is proposed in which the tension and compression overstrength factors, ω_T and ω_C, are measured and the unbalanced load factor, γ (Eq. 3), is calculated from a pair of nominally identical BRBs tested to the same near-fault loading protocol but with opposite direction. The strain hardening properties of stainless steel (SS) BRBs were observed to result in overstrength at maximum 1.5 times greater than A36 BRBs. Further, BRBs subjected to high strain rate, on average, gave an overstrength 1.2 times that of BRBs tested at typical pseudo-static rates (Fig. 6). Finally, the dual post-yield stiffness, isotropic hardening, and instantaneous strain rate functions (Eqs. 9 to12) added to the existing Menegotto-Pinto model (OpenSees *Steel02*) provided excellent correlation to experimental results for both SS and A36 BRBs tested either pseudo-statically or dynamically (Fig. 8).

ACKNOWLEDGMENTS

Funding for this research was provided by the California Department of Transportation under Contract No. 65A0358 with Dr. Charly Sikorsky as the project manager. The authors would like to thank CoreBrace, LLC for donating the test specimens.

REFERENCES

AISC. (2010). *Seismic provisions for structural steel buildings*. AISC 341, Chicago, IL

Di Sarno, L., Elnashai, A.S., Nethercot, D.A. (2002). "Comparison between seismic response characteristics of carbon steel and stainless steel." *Proc.*, 12th European Conf. Earthquake Eng., London, Paper No. 765.

Filippou, F., Popov, E., Bertero, V. (1983) "Effects of bond deterioration on hysteretic behavior of reinforced concrete joints." *Report No. UCB/EERC-83/19*, Earthquake Engineering Research Center, Univ. of Calif, Berkeley.

Kaufmann, E.J., Metrovich, B.R., Pense, A.W. (2001). "Characterization of cyclic inelastic strain behavior on properties of A572 Gr. 50 and A913 Gr. 50 rolled sections." *ATLSS Report No. 01-13,* Lehigh University, Bethlehem, PA.

Lanning, J., Benzoni, G., Uang, C.M. (2013). "The feasibility of using buckling-restrained braces for long-span bridges: Near-fault loading protocols and full-scale testing." *Report No. SSRP 13/17*. Dept. of Structural Engineering, Univ. of California, San Diego, La Jolla, Calif.

Lanning, J., Uang, C.M. (2014). "Full-scale BRB testing: Dynamic near-fault protocols." Online video clip. YouTube, Dec. 13, 2012, Web. Feb. 11, 2014.

Nordberg, H. (2004). "Note on the sensitivity of SSs to strain rate." *Research Report No. 04-.0-1,* AvestaPolarit Research Foundation.

Paul, S.K., Sivaprasad, S., Dhar, S., Tarafder, S. (2010). "Cyclic plastic deformation and cyclic hardening/softening behavior in 304LN stainless steel." *Theor. App. Fract. Mech.*, 54, 63-70.

Ravi K.G., Satish, S.R., Kalyanaraman, V. (2007). "Behaviour of frames with non-buckling bracings under earthquake loading." *J. Constr. Steel Research*, 63(2), 254-262.

Sabelli, R., Mahin, S., Chang, C., (2003). "Seismic demands on steel braced frame buildings with buckling-restrained braces." *Eng. Struct.*, 25(5), 655-666.